



CFD investigation of starvation behaviors in a grease lubricated EHL rolling contact

Shuo Zhang¹ · Georg Jacobs¹ · Seyedmohammad Vafaei¹ · Stephan von Goeldel¹ · Florian König¹

Received: 1 November 2022 / Accepted: 19 January 2023 / Published online: 20 March 2023
© The Author(s) 2023

Abstract

Nowadays, more than 90% of all rolling element bearings are grease lubricated. Grease releases oil to separate the contacting surfaces by forming a stable oil film, thus resulting a long service life of a bearing. The film thickness is usually calculated by assuming fully flooded conditions. However, if the amount of released oil is insufficient, the film thickness will be reduced, which is termed as starvation. Grease lubricated rolling bearings have the risk of starvation even at fairly moderate speeds, which implies a high risk of wear and bearing failure. To reduce this risk, an accurate starvation model to predict film thickness under starvation is needed. In this contribution, a new starvation model based on the CFD method is used. The effects of starvation on film thickness and surface deformation are analyzed. For starved condition, film thickness at contact sides still remains fully flooded but decreases around contact center line because of the spring-back resilience of the material. Meanwhile, with increasing speed, the maximum deformation increases.

CFD-Simulation von Starvation im fettgeschmierten EHL-Wälzkontakt

Zusammenfassung

Heutzutage sind mehr als 90% aller Wälzlager fettgeschmiert. Das Fett gibt Öl ab, um die Kontaktflächen zu trennen, indem es einen stabilen Ölfilm bildet, was zu einer längeren Lebensdauer des Lagers führt. Die Schmierfilmdicke wird normalerweise unter der Annahme von Vollschrimerung berechnet. Wenn die Menge des freigesetzten Öls jedoch nicht ausreicht, verringert sich die Schmierfilmdicke, was als Starvation bezeichnet wird. Bei fettgeschmierten Wälzlagern besteht die Gefahr des Starvation selbst bei relativ moderaten Drehzahlen, was ein hohes Risiko von Verschleiß und Lagerausfall mit sich bringt. Um dieses Risiko zu verringern, wird ein genaues Starvation-Modell zur Vorhersage der Schmierfilmdicke benötigt. In diesem Paper wird ein neues, auf der CFD-Methode basierendes Starvation-Modell verwendet. Die Auswirkungen des Starvation auf die Schmierfilmdicke und die Oberflächenverformung werden analysiert. Im Starvation bleiben die Kontaktseiten immer noch vollständig geschmiert, nimmt aber die Schmierfilmdicke um die Kontaktmittellinie herum aufgrund der Elastizität des Materials ab. Gleichzeitig nimmt die maximale Verformung mit zunehmender Geschwindigkeit zu.

1 Introduction

Nowadays, more than 90% of all rolling element bearings are grease lubricated [1]. When fresh grease is applied to a rolling element bearing, the rolling elements push the bulk grease to the sides of the rolling track in an initial “churning

phase” [2]. This phase typically takes no more than 24 h [3]. Thereafter, grease acts as a reservoir slowly releasing oil [4, 5], which is referred to as oil bleeding [2]. Consequently, in the rolling contacts an elastohydrodynamic lubricating (EHL) film is formed by bled oil separating the contacting surfaces [6].

Under fully flooded conditions, when the rolling contacts are sufficiently supplied with bled oil, the EHL film can reduce friction losses and prevent premature bearing failure by avoiding direct metal-to-metal contact. Conversely, when the amount of oil supplied to the contact inlet is insufficient, the EHL film thickness decreases, having the

✉ Shuo Zhang
shuo.zhang@imse.rwth-aachen.de

¹ Institute for Machine Elements and Systems Engineering, RWTH Aachen University, Schinkelstr. 10, 52062 Aachen, Germany

risk of metal to metal contact. This lubrication condition is referred to as starvation [27]. In grease lubricated rolling bearings, the fully flooded condition can only be maintained in the initial churning phase [1]. In this condition, the film thickness can be calculated by assuming the grease to be a homogeneous fluid with a shear thinning behavior [7–12]. In the bleeding phase, the film thickness can usually be estimated by the empirical EHL film thickness formula, e.g. Hamrock-Dowson equation [13], using base oil properties [1, 14, 15] if the bearing is assumed running under fully flooded conditions. However, the amount of bleeding oil is generally limited. As concluded by Lugt [2], an overall agreement is that grease lubricated bearings are generally running under starvation. The inlet of the EHL contacts cannot be supplied with sufficient oil and film thickness is reduced. Therefore, using the fully flooded assumption can lead to an overestimated film thickness, which may have a higher risk of wear and bearing failure. To reduce this risk, an accurate model to predict oil distribution and film thickness is needed.

Experiments show that in the vicinity of a starved contact, there is free lubricant at sides of the track but less in the center [16]. This results in an increase of pressure at the contact sides in comparison to the pressure under fully-flooded conditions [17]. Due to varying pressure distribution, the unexpected excessive load at contact sides cause local deformation of a bearing race way and subsequent yielding of case/core interface [18]. Consequently, the fatigue of rolling bearings is caused by this unexpected load distribution below the stressed surface [19]. Therefore, it is required to know the pressure distribution and surface deformation of the contacts under starved conditions. However, this correlation is not considered in the numerical investigations of starved contacts by Nogi [20, 21] and Fishcer et al. [22, 23].

In this contribution, a new proposed starvation model is used to investigate the contribution from the bleeding oil to a grease lubricated rolling contact. In this model, two oil side bands are used as the inlet boundary condition and the surface tension driven formation of a meniscus in front of the contact is simulated. Further, the effects of the oil depletion in front of the contact on the film formation and surface deformation in a starved EHL point contact can be investigated.

2 Fundamental of governing equations

The oil distribution around a rolling contact is represented by its phase fraction α [17, 22, 23]. To avoid the discontinuous and non-differentiable nature around the interface, the *isoAdvector* method proposed by Roenby et al. [24] is

Table 1 Parameters used for current CFD simulation

Lubricant Parameter	Value	Operation Parameter	Value
η_{oil}^0	0.0733 Pa · s	F_{aim}	47N
ρ_{oil}	822 kg/m ³	R_{ball}	9.525 mm
z	0.416	E_{stell}	207 GPa
σ	0.028	ν_{stell}	0.29
θ	25°	E_{disc}	75 GPa
η_{air}	1.723×10^{-5} Pa · s	ν_{disc}	0.22
ρ_{air}	1.114 kg/m ³	u	244.5 ~ 422.8 mm/s

used, in which α at each mesh cell i between two time steps can be determined by:

$$\alpha_i^{(t+\Delta t)} = \alpha_i^{(t)} - \frac{1}{V_i} \sum_{j \in B_i} s_{ij} \int_t^{t+\Delta t} \int_{F_j} H(\mathbf{x}, t) \mathbf{U}(\mathbf{x}, t) \cdot d\mathbf{S} dt \quad (1)$$

where V_i is mesh volume, F_j is mesh face of mesh cell i , $H(\mathbf{x}, t)$ is the indicator field. The only unknown in Eq. 1 is $\mathbf{U}(\mathbf{x}, t)$ is the velocity field, which can be determined by solving the Navier-Stokes equations for incompressible multi-phase fluid [25]:

$$\nabla \cdot \mathbf{U} = 0 \quad (2)$$

$$\frac{\partial \rho \mathbf{U}}{\partial t} + \nabla \cdot (\rho \mathbf{U} \mathbf{U}) - \nabla \cdot (\eta \nabla \mathbf{U}) - \nabla \mathbf{U} \cdot \nabla \eta = -\nabla p + \mathbf{g} \cdot \mathbf{h} \nabla \rho + \sigma \kappa \nabla \alpha \quad (3)$$

where ρ and μ are the density and viscosity of the oil/air mixture, respectively:

$$\eta = \alpha_{oil} \eta_{oil} + (1 - \alpha_{oil}) \eta_{air} \quad (4)$$

$$\rho = \alpha_{oil} \rho_{oil} + (1 - \alpha_{oil}) \rho_{air} \quad (5)$$

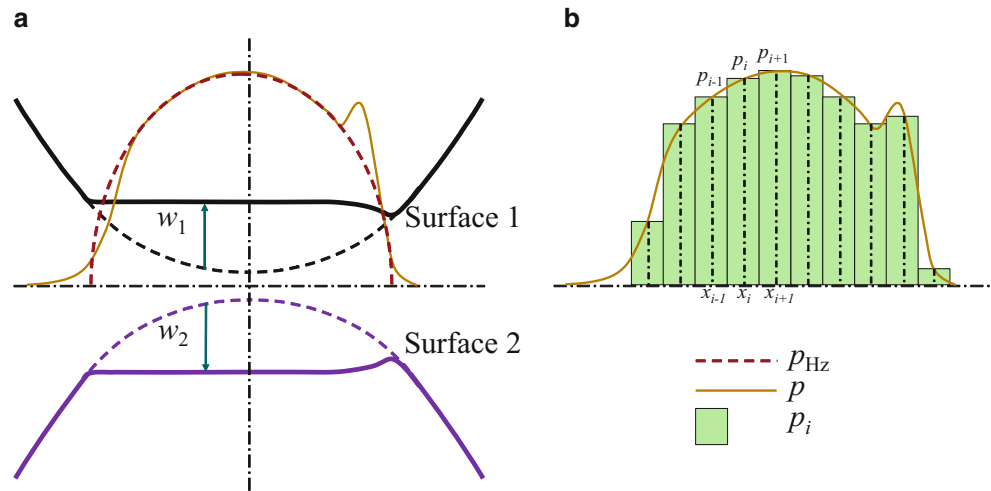
Lubricant and operation parameters are listed in Table 1. In this study, Roelands equation was used to model the pressure-viscosity relation [1]:

$$\eta_{oil} = \eta_{oil}^0 \cdot e^{\left\{ (\ln \eta_{oil}^0 + 9.67) \cdot \left[\left(1 + \frac{p}{p_{ref}} \right)^z - 1 \right] \right\}} \quad (6)$$

where η_{oil}^0 is the viscosity at ambient pressure, $p_{ref} = 1.96 \times 10^8$ Pa and z is the pressure-viscosity index.

Eqs. 1–6 are solved in the open source CFD package OpenFOAM by the GAMG matrix solver with DIC smoother [26]. The tolerances within each time step are set as 10^{-7} . After that, the pressure and velocity field can be

Fig. 1 Schematic of deformation calculation. **a** Pressure and deformation of two surfaces in an EHL contact **b** Pressure distribution approximated by zero-order shape function



obtained. Then, the rigid displacement increment Δh can be determined [27]:

$$\Delta h = \frac{\Delta t}{t_d} \cdot r_h \cdot (u_{\max} - u_{\min}) \frac{F_{\text{aim}} - F}{F_{\text{aim}}} \quad (7)$$

where F is the current load by integrating of pressure $p_{i,j}$ over deformable surface and F_{aim} is the target load.

When two surfaces in an EHL contact have different Young’s moduli E_1, E_2 and different Poisson’s ratios ν_1, ν_2 , the total elastic normal deformation w is the sum of those of the two contacting surfaces, as described in Fig. 1a. The w can be calculated by the Boussinesq integral of the displacement-pressure relationship [28]:

$$w = w_1 + w_2 = \frac{(1 - \nu_1^2)}{\pi E_1} \iint_{\Omega} \frac{p(\xi, \eta)}{\sqrt{(x - \xi)^2 + (z - \eta)^2}} d\xi d\eta + \frac{(1 - \nu_2^2)}{\pi E_2} \iint_{\Omega} \frac{p(\xi, \eta)}{\sqrt{(x - \xi)^2 + (z - \eta)^2}} d\xi d\eta = \left[\frac{(1 - \nu_1^2)}{\pi E_1} + \frac{(1 - \nu_2^2)}{\pi E_2} \right] \iint_{\Omega} \frac{p(\xi, \eta)}{\sqrt{(x - \xi)^2 + (z - \eta)^2}} d\xi d\eta \quad (8)$$

Generally, in the EHL simulation, the relationship in Eq. 8 is expressed as:

$$w = \frac{2}{\pi E'} \iint_{\Omega} \frac{p(\xi, \eta)}{\sqrt{(x - \xi)^2 + (z - \eta)^2}} d\xi d\eta \quad (9)$$

where the E' is termed as the reduced/effective Young’s modulus and calculated by:

$$E' = 2 \left(\frac{1 - \nu_{\text{stell}}^2}{E_{\text{stell}}} + \frac{1 - \nu_{\text{disc}}^2}{E_{\text{disc}}} \right)^{-1} \quad (10)$$

In a conventional way, the computational complexity can be reduced by constructing an influence coefficient matrix $D_{i,j}^{k,l}$. Thus, the nodal displacement vector $w_{k,l}$ can be reduced as the multiplication of $D_{i,j}^{k,l}$ and the nodal pressure vector $p_{i,j}$, as Eq. 11 [28, 29]:

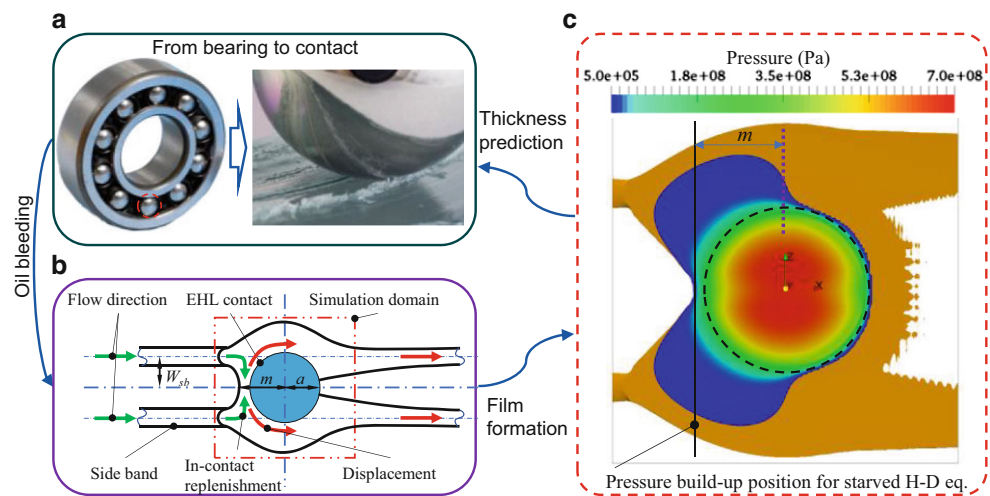
$$w_{k,l} = \frac{2}{\pi E'} \sum_{i=1}^n \sum_{j=1}^m D_{i,j}^{k,l} (p_{i,j}) \quad (11)$$

$(i, k = 1, 2 \dots n \text{ and } j, l = 1, 2 \dots m)$

where (i,j) is mesh index of fluid domain, (k,l) is mesh index in the solid domain, $w_{k,l}$ normal elastic deformation at mesh (k,l) , n and m are mesh number at x and z direction respectively (in this work, $n = m = 140$). In order to calculate $D_{i,j}^{k,l}$, the arbitrarily distributed pressure within each small mesh element was approximated by the zero-order shape function, as shown in Fig. 1b and introduced by Wang and Zhu [28].

To increase the model stability, an under-relaxation factor for pressure r_p between two timesteps is used and its value changes from 10^{-4} to 10^{-5} . When $F_{\text{error}} = |F_{\text{aim}} - F| / F_{\text{aim}} < 10^{-3}$, the simulation will be stopped. For the validation of this CFD model, the reader is referred to [17].

Fig. 2 Simplification of modelling a grease lubricated rolling contact. **a** From bearing to contact **b** Model of Oil distribution around a starved point contact. **c** Simulation domain in this work



3 Mesh model and boundary conditions

The simplification of modelling a grease lubricated rolling contact is shown in Fig. 2. The film formation of a grease lubricated bearing is often investigated using a ball-on-disk tribometer, as shown in Fig. 2a. As aforementioned, grease releases oil to the contact in bleeding phase. Unfortunately, until now there is no such a well-developed approach to determine the bleeding oil volume in the vicinity of grease lubricated rolling contacts. In this work, the oil volume is represented by the inlet cross-section area. A higher cross-section area means more oil entering into the vicinity of the contact. Meanwhile, a deposited thickener layer may be formed on the rolling track [30], which changes the contact angle between contact surfaces [31]. To include this effect, the cross-section area is set with a specified contact angle [17].

As shown in Fig. 2b, the flow in front of the contact has two side bands from the outlet of the previous rolling element. In the vicinity of the contact, the side bands are affected by the converging gap between the contacting surfaces [20, 23]. The part of oil replenishes ball-raceway contact and results in a so-called butterfly shape of oil flow

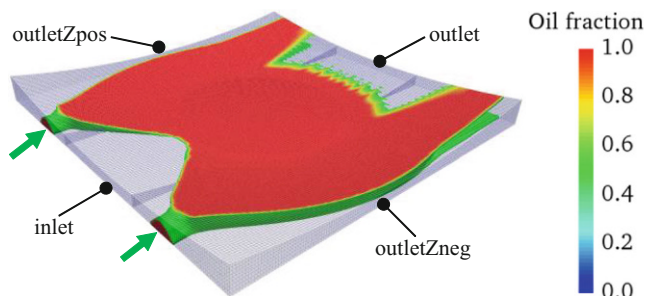


Fig. 3 Mesh model and boundaries of the CFD model (The color indicates the oil fraction)

with a concave air/oil meniscus in front of the rolling contact [32–34]. It has been experimentally [14] and numerically [35] shown that replenishment is a close-to-contact phenomenon and is negligible on the tracks between overrollings. And grease lubricated rolling bearings have the risk of starvation even at fairly moderate speeds [36]. Therefore, the simulation domain in present work is only limited to the field around a contact, as shown in Fig. 2c.

The geometry of a deformable ball surface against a rigid plane is simulated in this work, as shown in Fig. 2c and Fig. 3. The *fixedValue* and *rotatingWallVelocity* conditions are specified for the velocity of the rigid plane and the deformable ball surface, respectively. The other four boundaries marked in Fig. 3 are connected with atmosphere so needs to permit both outflow and inflow according to the flow within the simulation domain. Therefore, a combination of boundary conditions is used to do this and maintain the stability [26]. In this work, the combination is *pressureInletOutletVelocity* for velocity and *totalPressure* for pressure [26]. The specified total pressure is 0 Pa.

The critical meniscus distance m^* is a value to determine the onset of starvation [21, 22], which is proposed by Hamrock and Dowson [37], and can be calculated by Eq. 12:

$$m^* = \left[1 + 3.06 * \left(h_{ff,c} * \frac{R_{ball}}{a^2} \right)^{0.58} \right] * a \quad (12)$$

where $h_{ff,c}$ is the central film thickness calculated by the fully flooded Hamrock-Dowson equations [13]. If the meniscus in front of a contact is less than m^* , starvation occurs. For all simulation cases in this work, $1.38a \leq m^* \leq 1.58a$. To ensure that starvation is not affected by the model size [17], the model size in both flow and cross-flow direction should always be bigger than m^* and is therefore set to $2a$.

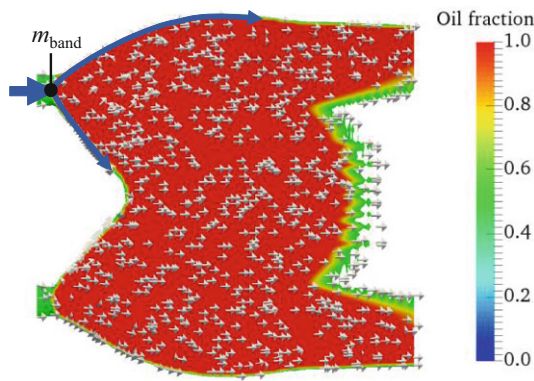


Fig. 4 Oil distribution and velocity at $u = 361.7 \text{ mm/s}$ (velocity is indicated by white arrows)

4 Results and discussion

In the following, the effects of starvation on the film thickness and the surface deformation are analyzed by comparing the results under fully flooded and starved conditions. After this, the results with various rolling speeds are compared to show the effects of replenishment on the pressure distribution and the surface deformation.

4.1 Effects of starvation on film thickness

To elucidate the EHL film formation in a starved rolling contact, the oil distribution and velocity field for a rolling speed at $u = 361.7 \text{ mm/s}$ are shown in Fig. 4. The arrows represent the velocity field of flow. The inlet oil has two side flow bands from the outlet of the previous rolling element. In front of the contact, side bands separate after filling the contact clearance at oil band meniscus position (m_{band}). As indicated by the arrows direction, part of the oil flows transversely to the center region by the capillary forces/surface tension force [35] and then is dragged into the concentrated ball-raceway contact by the rolling surfaces to replenish the

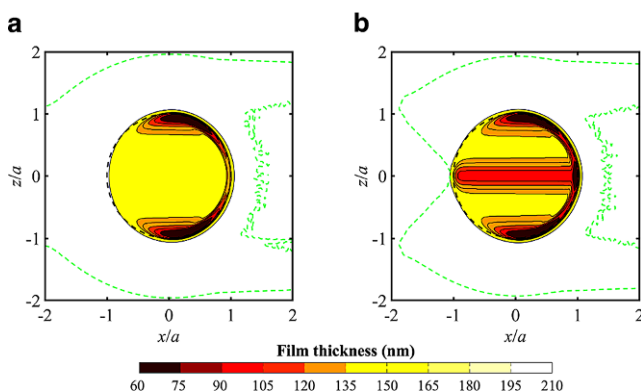


Fig. 5 Comparison of the film thickness at $u = 361.7 \text{ mm/s}$ (green line indicates the interface of oil and air) **a** fully flooded condition **b** starved condition

contact. This flow is referred to as in-contact replenishment from side bands, which results in a concave meniscus in front of the contact. This oil distribution field agrees well with the simulation results by Fischer et al. [22, 23], in which the film thickness is assumed as a fixed value.

The meniscus (indicated by green dotted lines) and the film thickness profiles are plotted together in Fig. 5. For the fully flooded condition (Fig. 5a), the EHL film thickness is the classical and well-known “horseshoe” shape [16]. The minimum film thickness appears at the rear and sides of the contact, while the film thickness at contact center is almost constant. Comparing Fig. 5a,b, the film thickness at contact sides under the fully flooded condition and starved condition are similar. In contrast, a decreasing film thickness around contact center line ($z/a = 0$) can be observed. This film thickness reduction will be analyzed in the next section. This starved film thickness distribution agrees with the experimental observations of the starved oil lubrication [38, 39] and the grease lubrication [16].

4.2 Effects of starvation on contact pressure and deformation

To show how the pressure build-up is restricted by the meniscus in front of the contact, the meniscus and pressure distribution are shown together in Fig. 6. For the fully flooded condition, there is sufficient oil presenting in front of the contact. Hence, the meniscus is absent in the simulation domain. The pressure build-up starts relatively far upstream to the contact and with a near-zero pressure gradient. Therefore, the typical pressure distribution of an EHL point contact with the maximum pressure at the contact center can be observed. In contrast, the starved pressure build-up can only begin after the meniscus, which is closer to the Hertzian contact with a non-zero pressure gradient. Moreover, the pressure map is obviously separated into two parts by $z/a = 0$, due to insufficient oil supply into the contact center.

A fast and simple way to evaluate the potential lifetime of a rolling contact is to treat the rolling contact as a Hertzian dry contact [19]. Therefore, in the following, the pressure and surface deformation from CFD-based simulations are compared with the results from the Hertzian theory. According to the Hertzian theory, the contact area for a ball against the rigid surface is flat. Therefore, a relative deformation to the Hertzian contact is used in postprocess, which is defined as:

$$w_{Hzk,l} - w_{k,l} = \frac{2}{\pi E'} \sum_{i=1}^n \sum_{j=1}^m D_{i,j}^{k,l} (p_{Hzi,j} - p_{i,j}) \quad (13)$$

where $w_{Hzk,l}$ elastic deformation caused by the Hertzian dry contact pressure $p_{Hzi,j}$.

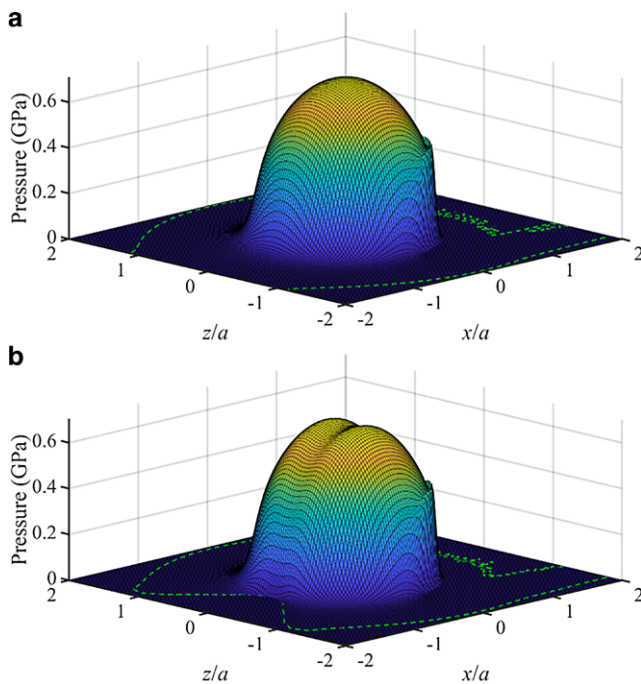


Fig. 6 Comparison of pressure at $u=361.7$ mm/s (green line indicates the interface of oil and air) **a** fully flooded condition **b** starved condition

In this way, the positive value by Eq. 13 means a contraction, thereby a thinner film thickness, whereas a negative value means a thicker film thickness. The contact surface deformation can be clearly shown with the 3D deformation map in Fig. 7. For the fully flooded condition, the pressure builds up the second peak just before the minimum film thickness point. Behind the peak, the pressure drops abruptly back to ambient pressure values. Due to the spring-back resilience of the material, the contraction occurs at the sides and rear of the contact. The second pressure peak and contraction are two important features of the fully flooded condition [29]. However, this contraction becomes inconspicuous under the starved condition. Here, a contraction is found at the contact center under starvation. This is because the pressure here is limited by the concave meniscus in front of the contact, as shown in Fig. 6b.

4.3 Effects of replenishment on contact deformation

According to the numerical results from Nogi et al. [21] and Fischer et al. [23], the in-contact replenishment is controlled by the capillary number, which is defined as the viscous forces ($\eta_{oil}^0 \cdot u$) divided by the surface tension force σ . With increasing rolling speeds, the viscous forces dominate over the surface tension force. Therefore, less replenishment results in a decrease of the meniscus distance. As shown in Fig. 8, the meniscus advances the Hertzian radius from $u=244.5$ mm/s to $u=361.7$ mm/s. At $u=244.5$ mm/s,

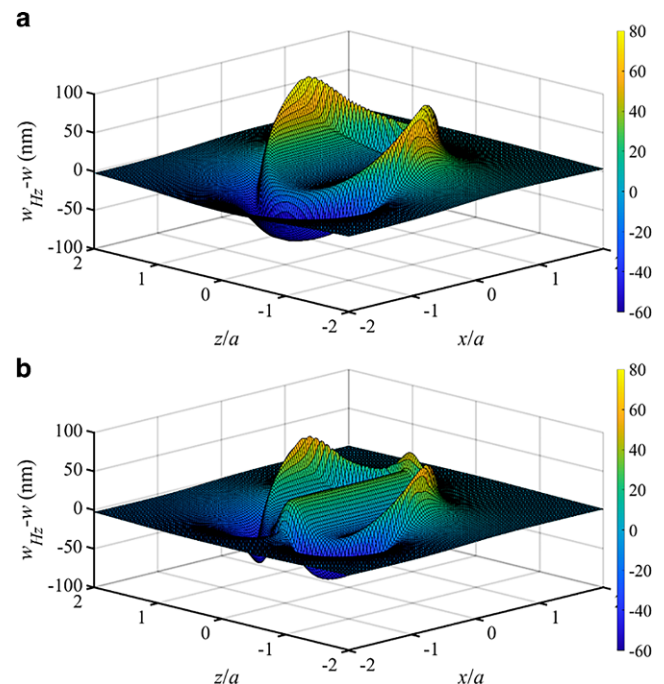


Fig. 7 Comparison of the deformation at $u=361.7$ mm/s **a** fully flooded condition **b** starved condition

the meniscus is far away from the contact center and $m/a = 1.563$, which is bigger than the critical value $m^*/a = 1.460$. Therefore, the condition is still fully flooded. With a further increase of speed to $u=309.4$ mm/s, starvation occurs. At $u=391.1$ mm/s, a convex meniscus presents in front of the contact. Therefore, severe starvation occurs and the starved zone expands to the sides, hindering the pressure build-up at the center line ($z/a=0$).

The pressure difference is shown in Fig. 9 for various speeds. At $u=244.5$ mm/s, the lubrication condition still remains fully flooded and the maximum pressure happens at contact center. After starvation occurs, the pressure difference has two pressure zones within the Hertzian contact, a high-pressure zone around $z/a = \pm 0.5$ and a weak pressure zone at the contact center around $z/a = 0$. With an increasing of rolling speeds, the pressure at the high-pres-

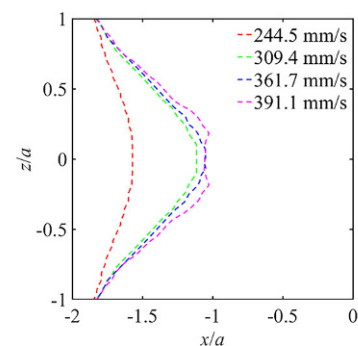


Fig. 8 Meniscus in front of contact for various rolling speeds

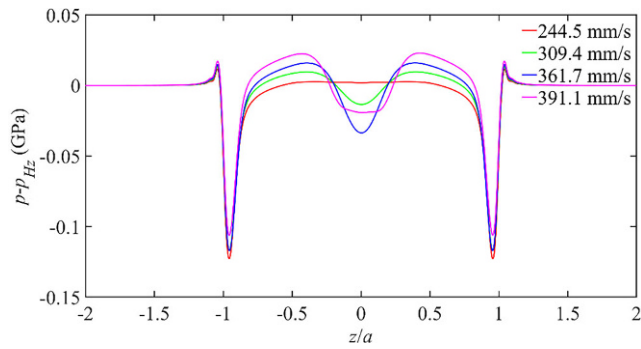


Fig. 9 Comparison of pressure for various rolling speeds at $x/a=0$

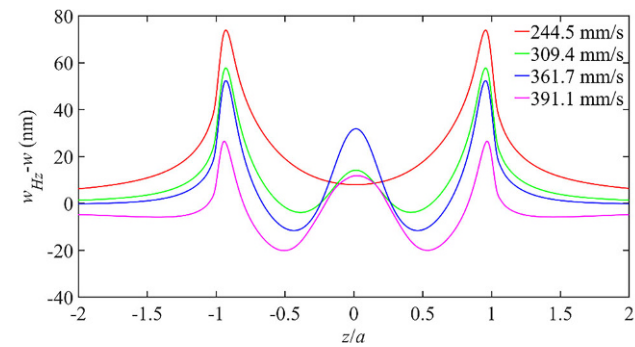
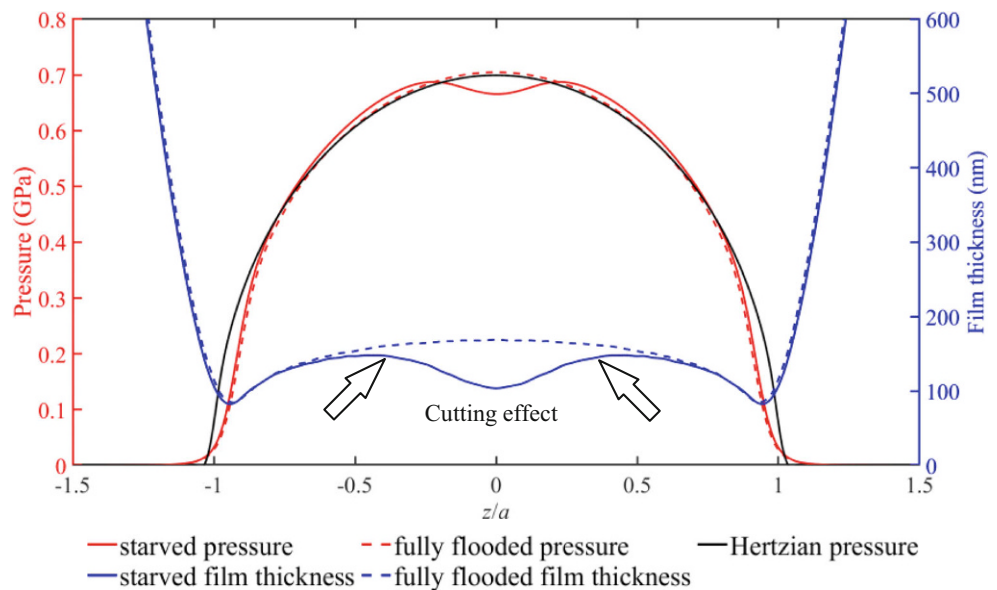


Fig. 10 Comparison of deformation for various rolling speeds at $x/a=0$

sure zone increases. This observation can be linked to the fact that the meniscus around $z/a = \pm 0.5$ is still far away from the contact center. An increasing speed leads to an enhancement of the hydrodynamic effects, which leads to an increased pressure around ± 0.5 .

Since the side bands still replenish the contact to some extent, the contact side can contribute towards EHL film

Fig. 11 Pressure and film thickness at $x/a=0$ and $u=361.7$ mm/s



formation and load-carrying capacity. Consequently, the starved pressure at contact center is always smaller than the Hertzian dry contact pressure. However, at the contact center, the meniscus approaches to the Hertzian contact circle. Therefore, from $u=244.5$ to 361.7 mm/s, the pressure keeps decreasing. With a further increase of speed to $u=391.1$ mm/s, less oil is replenished. The starved zone increases further, as indicated by a convex meniscus at the contact center in Fig. 8. In this case, pressure around $z/a = 0$ increases to carry the same load as $u=361.7$ mm/s.

Due to the uneven pressure distribution at different degrees of starvation, different surface deformations are expected. The relative surface deformations compared to the Hertzian contact at various rolling speeds are shown in Fig. 10. At $u=244.5$ mm/s, the maximum deformation ($w_{Hz} - w = 8nm$) happens at the contact center where the maximum pressure happens. With a further increase of the speed to $u=309.4$ mm/s, the higher pressure around $z/a = \pm 0.5$ leads to higher surface deformation ($w_{Hz} - w = -3.9nm$) and a deeper valley is formed at $z/a = \pm 0.385$. Increasing speed to $u=361.7$ mm/s, leads to an increase of maximum deformation to $w_{Hz} - w = -11.6nm$ at $z/a = \pm 0.464$. For $u=391.1$ mm/s, maximum deformation to $w_{Hz} - w = -20.1nm$ at $z/a = \pm 0.506$.

In addition to the deformation, the pressure and film thickness are compared under fully flooded and starved condition, as shown in Fig. 11. Comparing with the fully flooded condition, the starved pressure is restricted at $z/a = 0$ and the center film thickness decreases about $62nm$ (-37%). The deformation and pressure are wavier under starvation. The Mises stress in the surface-near region or the subsurface region become very high when the surface is wavier as introduced by Wang and Zhu [28]. Therefore, the fatigue limits may be exceeded. Meanwhile,

surface initiated fatigue is most likely to appear when the surface irregularities, like stretches and indentations, are presented [40]. After micro cracks formed, the high pressure in the valley would promote the crack expansion. Therefore, a cutting effect happens to the contraction at the contact center under starvation, which may lead to a fatigue damage at the contact center. However, for the subsurface stress in the starved rolling contact, further investigation should be performed.

5 Conclusion

In grease lubricated rolling contacts, bleeding oil has a dominant contribution to film thickness. At high rolling speeds, less bled oil is replenished than displaced, which leads to starvation and decrease of the film thickness. To reduce risk of severe metal-to-metal contact, it is essential to ensure a sufficient oil film to separate contacting surfaces. Considering the replenishment, this work presents a two-phase flow model based on CFD method to predict the flow field in the vicinity of the contact and its effect on the film thickness and surface deformation. The results are concluded as follows.

1. The film thickness at contact sides under the fully flooded condition and starved condition are similar. In contrast, the film thickness under starvation decreases at the contact center.
2. Under starved condition, the pressure separates into a higher-pressure zone and a weak-pressure zone. Unlike the film thickness under the fully flooded condition, the contraction occurs at the contact center in flow direction under starvation, because of the spring-back resilience of the material.
3. The analysis of the effects by replenishment on the surface deformation reveal that with an increasing speed, the maximum deformation and the waviness of the pressure profile increases, thereby inducing a so-called cutting effect, which may lead to fatigue-critical stress conditions at the contact center.

The presented CFD-model helps to investigate on the starvation behaviors in a grease lubricated EHL rolling contact. Further work will focus on the influence of the different parameters on the film thicknesses. Those parameters can be classified into three groups, lubricant supply related parameters, replenishment related parameters and contact related parameters. The first group includes contact angle and bleeding oil volume. The second group includes oil viscosity, rolling speed and surface tension coefficient. The third group includes contact load, contact radius and ellipticity ratio. Considering the time-efficiency requirements in industrial bearing design, empirical equations correlating

Table 2 Nomenclature

Symbol	Description	Unit
a	Hertzian radius, = 1.791×10^{-3} in this work	m
B_i	Boundary of mesh cell i	–
Ca	Capillary number	–
$D_{i,j}^{k,l}$	Influence coefficient matrix	–
E'	Reduced/effective Young's modulus	GPa
$E_{\text{stell}}, E_{\text{disc}}$	Elastic modulus of ball and disc	GPa
$\nu_{\text{stell}}, \nu_{\text{disc}}$	Poisson ratio of ball and disc	–
F_j	Face j of mesh cell i	–
F	Force generated by EHL contact	N
F_{aim}	Applied force	N
$H(\mathbf{x}, t)$	Indicator field at position \mathbf{x} and time t , = $\rho(\mathbf{x}, t) - Q_{\text{air}} / Q_{\text{oil}} - Q_{\text{air}}$	–
H_{ffc}	Fully flooded central film thickness	m
$\mathbf{U}(\mathbf{x}, t)$	Velocity field at position \mathbf{x} and time t	$\text{m} \cdot \text{s}^{-1}$
u	Rolling speed	$\text{mm} \cdot \text{s}^{-1}$
V_i	Volume of mesh cell i	m^3
m^*	Critical meniscus distance	m
p	EHL Pressure	Pa
p_{Hz}	Hertzian dry contact pressure	Pa
R_{ball}	Radius of ball	mm
R_p	Under-relaxation factor of pressure	–
\mathbf{S}	Surface area direction vector	–
S_{ij}	Auxiliary factor, = +1 or –1	–
w_{Hz}	Flattening by Hertzian pressure	m
z	Pressure-viscosity index	–
α_i	O _i volume fraction of mesh cell i	–
η_{oil}^0	Viscosity of oil at ambient pressure	Pa · s
η_{air}	Viscosity of air	Pa · s
$Q_{\text{oil}}, Q_{\text{air}}$	Density of oil and air	$\text{kg} \cdot \text{m}^{-3}$
σ	Surface tension coefficient	–
θ	Contact angle	°

those parameters with film thickness will be formulated by parameter study.

6 Nomenclature

The nomenclature is shown in Table 2.

Acknowledgements The author Shuo Zhang thanks China Scholarship Council, China (No. CSC202006450015) for supporting this work. Simulations were performed with computing resources granted by RWTH Aachen University under project ID rwth0910.

Funding Open Access funding enabled and organized by Projekt DEAL.

Open Access This article is licensed under a Creative Commons Attribution 4.0 International License, which permits use, sharing, adaptation, distribution and reproduction in any medium or format, as long as

you give appropriate credit to the original author(s) and the source, provide a link to the Creative Commons licence, and indicate if changes were made. The images or other third party material in this article are included in the article's Creative Commons licence, unless indicated otherwise in a credit line to the material. If material is not included in the article's Creative Commons licence and your intended use is not permitted by statutory regulation or exceeds the permitted use, you will need to obtain permission directly from the copyright holder. To view a copy of this licence, visit <http://creativecommons.org/licenses/by/4.0/>.

References

- Lugt PM (2013) Grease lubrication in rolling bearings. Tribology in practice series. Wiley-Blackwell, Chichester
- Lugt PM (2009) A review on grease lubrication in rolling bearings. Tribol Trans 52:470–480. <https://doi.org/10.1080/10402000802687940>
- Cyriac F, Lugt PM, Bosman R et al (2016) Effect of thickener particle geometry and concentration on the grease EHL film thickness at medium speeds. Tribol Lett 61:470. <https://doi.org/10.1007/s11249-015-0633-z>
- Cann P (1996) Understanding grease lubrication. Tribol Ser 31:573–581. [https://doi.org/10.1016/S0167-8922\(08\)70819-8](https://doi.org/10.1016/S0167-8922(08)70819-8)
- Huang L, Guo D, Wen S (2014) Starvation and reflow of point contact lubricated with greases of different chemical formulation. Tribol Lett 55:483–492. <https://doi.org/10.1007/s11249-014-0376-2>
- Huang L, Guo D, Shizhu W (2016) Film thickness decay and replenishment in point contact lubricated with different greases: A study into oil bleeding and the evolution of lubricant reservoir. Tribol Int 93:620–627. <https://doi.org/10.1016/j.triboint.2014.11.005>
- Bordenet L, Dalmaz G, Chaomleffel J-P et al (1990) A study of grease film thicknesses in elastohydrodynamic rolling point contacts. Lubr Sci 2:273–284. <https://doi.org/10.1002/lr.3010020402>
- Karthikeyan BK, Teodorescu M, Rahnejat H et al (2010) Thermoe-elastohydrodynamics of grease-lubricated concentrated point contacts. Proc Inst Mech Eng Part C J Mech Eng Sci 224:683–695. <https://doi.org/10.1243/09544062JMES1748>
- Mubashshir M, Shaikat A (2019) The role of grease composition and rheology in elastohydrodynamic lubrication. Tribol Lett 67:1085. <https://doi.org/10.1007/s11249-019-1218-z>
- Kakoi K (2021) Formulation to calculate isothermal, non-newtonian elastohydrodynamic lubrication problems using a pressure gradient coordinate system and its verification by an experimental grease. Lubricants 9:56. <https://doi.org/10.3390/lubricants9050056>
- Wang D, Yang J, Wei P et al (2021) A mixed EHL model of grease lubrication considering surface roughness and the study of friction behavior. Tribol Int 154:106710. <https://doi.org/10.1016/j.triboint.2020.106710>
- Nogi T, Soma M, Dong D (2020) Numerical analysis of grease film thickness and thickener concentration in elastohydrodynamic lubrication of point contacts. Tribol Trans 63:924–934. <https://doi.org/10.1080/10402004.2020.1778147>
- Hamrock BJ, Dowson D (1977) Isothermal elastohydrodynamic lubrication of point contacts: part III—Fully flooded results. J Lubr Technol 99:264–275. <https://doi.org/10.1115/1.3453074>
- Cen H, Lugt PM (2020) Replenishment of the EHL contacts in a grease lubricated ball bearing. Tribol Int 146:106064. <https://doi.org/10.1016/j.triboint.2019.106064>
- Zerwas T, Jacobs G, Kowalski J et al (2022) Model signatures for the integration of simulation models into system models. Systems 10:199. <https://doi.org/10.3390/systems10060199>
- Cann PME (1999) Thin-film grease lubrication. Proc Inst Mech Eng Part J J Eng Tribol 213:405–416. <https://doi.org/10.1243/1350650991542776>
- Zhang S, Jacobs G, von Goedel S et al (2023) Prediction of film thickness in starved EHL point contacts using two-phase flow CFD model. Tribol Int 178:108103. <https://doi.org/10.1016/j.triboint.2022.108103>
- Starvin MS, Babu S, Aithal S et al (2013) Finite element simulation of non-linear deformation behaviour in large diameter angular contact thrust bearing vol 8, pp 128–138 <https://doi.org/10.5897/SRE12.536>
- Harris TA, Kotzalas MN (2007) Rolling bearing analysis: Essential concepts of bearing technology, 5th edn. CRC, Boca Raton
- Nogi T (2015) An analysis of starved EHL point contacts with reflow. Tribol Online 10:64–75. <https://doi.org/10.2474/trol.10.64>
- Nogi T (2015) Film thickness and rolling resistance in starved elastohydrodynamic lubrication of point contacts with reflow. J Tribol 137:6. <https://doi.org/10.1115/1.4030203>
- Fischer D, von Goedel S, Jacobs G et al (2021) Investigation of lubricant supply in rolling point contacts under starved conditions using CFD simulations. IOP Conf Ser: Mater Sci Eng 1097:12007. <https://doi.org/10.1088/1757-899X/1097/1/012007>
- Fischer D, von Goedel S, Jacobs G et al (2021) Numerical investigation of effects on replenishment in rolling point contacts using CFD simulations. Tribol Int 18:106858. <https://doi.org/10.1016/j.triboint.2021.106858>
- Roenby J, Bredmose H, Jasak H (2016) A computational method for sharp interface advection. R Soc Open Sci 3:160405. <https://doi.org/10.1098/rsos.160405>
- Damian SM (2013) An extended mixture model for the simultaneous treatment of short and long scale interfaces
- Greenshields CJ, Weller HG (2022) Notes on computational fluid dynamics: General principles. CFD Direct Limited, Reading
- Hajishafiee A, Kadirci A, Ioannides S et al (2017) A coupled finite-volume CFD solver for two-dimensional elasto-hydrodynamic lubrication problems with particular application to rolling element bearings. Tribol Int 109:258–273. <https://doi.org/10.1016/j.triboint.2016.12.046>
- Wang Q, Zhu D (eds) (2019) Interfacial mechanics: Theories and methods for contact and lubrication, 1st edn. CRC Press, Boca Raton
- Wen S, Huang P (2017) Principles of tribology, 2nd edn. Tsinghua University Press, Beijing
- Cann PME, Lubrecht A, Venner CH (eds) (2000) Grease lubrication of rolling element bearings—A model future?
- Huang L, Guo D, Liu X et al (2016) Effects of nano thickener deposited film on the behaviour of starvation and replenishment of lubricating greases. Friction 4:313–323. <https://doi.org/10.1007/s40544-016-0123-9>
- Huang L, Guo D, Wen S et al (2014) Effects of slide/roll ratio on the behaviours of grease reservoir and film thickness of point contact. Tribol Lett 54:263–271. <https://doi.org/10.1007/s11249-014-0301-8>
- Chen J, Tanaka H, Sugimura J (2015) Experimental study of starvation and flow behavior in grease-lubricated EHD contact. Tribol Online 10:48–55. <https://doi.org/10.2474/trol.10.48>
- Sakai K, Kostal D, Shitara Y et al (2017) Influence of Li grease thickener types on film thicknesses formed between smooth and dented surfaces. Tribol Online 12:262–273. <https://doi.org/10.2474/trol.12.262>
- Jacod B, Pubilier F, Cann PME et al (1999) An analysis of track replenishment mechanisms in the starved regime. Tribol Ser 36:483–492. [https://doi.org/10.1016/S0167-8922\(99\)80069-8](https://doi.org/10.1016/S0167-8922(99)80069-8)
- Cen H, Lugt PM (2019) Film thickness in a grease lubricated ball bearing. Tribol Int 134:26–35. <https://doi.org/10.1016/j.triboint.2019.01.032>
- Hamrock BJ, Dowson D (1977) Isothermal elastohydrodynamic lubrication of point contacts: part IV—Starvation results. J Lubr Technol 99:15–23. <https://doi.org/10.1115/1.3452973>

38. Chevalier F, Lubrecht AA, Cann PME et al (1998) Film thickness in starved EHL point contacts. *J Tribol* 120:126–133. <https://doi.org/10.1115/1.2834175>
39. Popovici G (2005) Effects of lubricant starvation on performance of elasto-hydrodynamically lubricated contacts
40. Sadeghi F, Jalalahmadi B, Slack TS et al (2009) A review of rolling contact fatigue. *J Tribol*. <https://doi.org/10.1115/1.3209132>